

Exploration of Dependence of Organo-Catalyzed Enantioselective Michael Addition on the Pore Size of Mesoporous Host

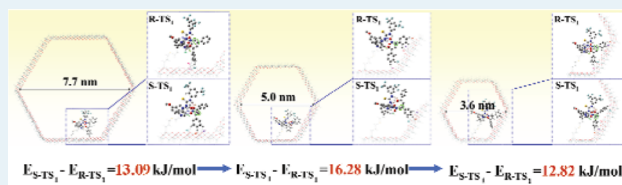
Liwei Zhao, Yaping Li, Peng Yu, Xu Han, and Jing He*

State Key Laboratory of Chemical Resource Engineering, Beijing University of Chemical Technology, Beijing 100029, China

Supporting Information

ABSTRACT: Confinement, an effective strategy to improve the enantioselectivity in metal-catalyzed asymmetric synthesis, is a great challenge to the heterogeneous organocatalysis via hydrogen-bonding activation in that hydrogen bonding is more sensitive to the complicated spatial or chemical microenvironment in confined spaces. Here, visible improvement of enantioselectivity has been experimentally achieved on heterogeneous 9-amino (9-deoxy) epiquinine and 9-thiourea epiquinine catalysts in the Michael addition by rationally modulating the pore size of the mesoporous host. The enantiomer excess for heterogeneous 9-thiourea epiquinine is level with the homogeneous counterpart when the support pore size is reduced to an optimized spatial dimension. Theoretical calculations revealed that the immobilization can switch the activation routes, and the hydrogen-bonding interaction between substrate and pore wall influences the energy gap between *R/S* transition states, well accounting for the dependence of enantioselectivity on the pore size experimentally observed in the heterogeneous organocatalytic Michael addition. The results not only demonstrate significant development in the comprehension of confinement in the heterogeneous asymmetric catalysis but also suggest an original strategy in designing efficient enantioselective heterogeneous catalysts.

KEYWORDS: confinement, organocatalysis, enantioselectivity, heterogeneous catalysis, hydrogen-bonding interaction



1. INTRODUCTION

The growing demand in the pharmaceutical and agrochemical industries for efficient and economical synthetic routes to enantiomerically pure compounds has focused much attention on heterogeneous asymmetric catalysis and catalysts,^{1,2} but binding a homogeneous catalyst to solid surfaces usually has led to a deteriorated activity.³ In the case of asymmetric catalysis, a visible reduction or even elimination of enantioselectivity often be observed.^{4–8} Encouraging success has been made in a few metal-complex-catalyzed asymmetric reactions^{9–15} to avoid the loss of enantioselectivity caused by the heterogenization or even enhancing the enantioselectivity through constraining the asymmetric catalytic moieties into confined spaces. For Rh^I complexes immobilized in mesoporous silica, for example, a gradual increase in the enantiomer excess with reduced pore size was observed in addition to a superior enantiomer excess in the asymmetric hydrogenation of methyl benzoylformate, whereas the homogeneous chiral catalyst gave the racemic products.¹⁶

The confinement effects realized in heterogeneous chiral ligand–metal complex catalysis have been qualitatively explained using two concepts.^{15,17} Thomas et al.¹⁷ proposed it was the constraints imposed by the space surrounding the metal center (active site) that dominated the enantioselectivity. The substrate's interaction with both the chiral directing group and the pore wall in the confined space contribute to influence the orientation of the substrate relative to the reactive catalytic center. Jones et al.¹⁵ later proposed it was the restricted access (to the active site by the relatively bulky reactants) generated

by the concavity of the pore that was the principal determinant of the enhancement of the ee values.

For most chiral reactions, however, the energy difference between *R* and *S* transition states is so small that the interference from the host surface, such as spatial restriction and interactions, could impose adverse effects on the enantioselectivity.¹⁸ For example, reduced ee was observed for the cyclopropanation of styrene with ethyl diazoacetate catalyzed by the copper-bis(oxazoline) immobilized inside mesoporous channels when compared with the homogeneous counterpart.¹⁹ Similar results were found on the chiral Mn(salen) catalyst grafted in the nanopores of MCM-41 in the asymmetric epoxidation of 1-phenylcyclohexene.²⁰ Moreover, in many cases, the enantioselectivity was found to decrease with reduced pore size.^{21–27} More remarkably, the confinement, effective in metal complex catalysis, encounters a great challenge when applied in organocatalysis in that not only is the organocatalysis much more sensitive to the spatial and chemical microenvironment,^{28,29} but also the organocatalysts are more prone to suffer from modification or alteration in the immobilization.³⁰ To improve the enantioselectivity of heterogeneous asymmetric organocatalysis by confinement is believed to be of more significance owing to its ease of manipulation, escape of metal contamination, and other merits,

Received: November 14, 2011

Revised: March 17, 2012

Published: April 24, 2012

as well as its potential application in a broad range of chiral synthesis.^{31–33}

The enantioselective Michael addition reaction, which represents the mechanism through hydrogen-bonding activation, is considered to be one of the most important methods for the construction of optically active compounds that are useful intermediates for a variety of natural and nonnatural products.^{34–36} Hydrogen-bonding activation, combining supramolecular recognition with chemical transformations in an environmentally benign fashion, has been recognized as a powerful activation mode in organocatalysis.^{37,38} Promising results have been observed for the heterogeneous hydrogen-bonding activation asymmetric organocatalysis,³⁹ but a much greater challenge could be predicted for implementation of confinement in hydrogen-bonding activation organocatalysis than covalent activation, such as enamine or imine activation organocatalysis, because the energy of hydrogen bonding is almost in the same range as the energy difference between the *R* and *S* transition states.¹⁸ Nevertheless, here, this work demonstrates that the adverse interference²⁹ of the support surface on the asymmetric organocatalysis via hydrogen-bonding activation can be eliminated successfully by modulating the size of the confined space. The experimental observations have been rationally interpreted with theoretical study by colligating the curvature of the support pore with the multiple hydrogen-bonding interactions. The results and conclusions in this work show valuable insight into the essence, as well as the applicability and practicability, of confinement strategy in enantioselective catalysis and asymmetric synthesis.

2. EXPERIMENTAL AND COMPUTATIONAL DETAILS

2.1. Materials and Methods. Tetraethyl orthosilicate (TEOS, 98%), triblock organic copolymer (EO₂₀-PO₇₀-EO₂₀) (Pluronic P123, Aldrich), trimethylchlorosilane (TMCS, 98%, Alfa Aesar), 3-mercaptopropyl-trimethoxysilane (MPTMS, 95%, Alfa Aesar), quinine (98%, Alfa Aesar), 3,5-bis-(trifluoromethyl)phenylisothiocyanate (99%, Matrix Scientific), diisopropyl azodicarboxylate (DIAD, 94%, Alfa Aesar), and diphenyl phosphoryl azide (DPPA, 97%, Alfa Aesar) were used as received without further purification. Other chemicals used in this work are all of analytical purity. Toluene and tetrahydrofuran (THF) were first dehydrated for 2 d by 0.4 nm zeolite and then distilled from a sodium/benzophenone system prior to use. Dichloromethane was distilled under N₂ atmosphere after being refluxed with CaH₂ for ~4 h. The dehydration by 0.4 nm zeolite was performed for 2 d, as well, before refluxing. Chiral 9-amino(9-deoxy)epiquinine was synthesized from quinine following a procedure described previously,⁴⁰ yielding 56.8–58.6%. 9-Thiourea epiquinine was prepared through the reaction of chiral 9-amino(9-deoxy)-epiquinine with 3,5-bis (trifluoromethyl)phenyl isothiocyanate in anhydrous THF, yielding 80.2–90.1%. MCM-41, synthesized following the procedure reported by Monnier et al.⁴¹ afforded the support materials with a pore size of 4.7 nm. SBA-15, synthesized following the procedure reported by Zhao et al.⁴² afforded support materials with pore sizes of 5.8, 6.3, 7.3, 9.8, 10.7, and 11.3 nm.

The grafting of trimethylsilyl groups was performed on the as-synthesized mesoporous materials to shelter the silanol groups at the exterior surface. Typically, 1.0 g of as-synthesized mesoporous material was first desiccated under vacuum at 50 °C and then mixed with 20 mL of anhydrous toluene under N₂ atmosphere. After 15 min of agitation, 66 μL of TMCS was

introduced. After 20 h of agitation at 80 °C, the solid was washed successively with toluene, hexane, and anhydrous ethanol and then dried under ambient temperature. A 0.5 g portion of sheltered support was suspended in a mixture of 128 mL of absolute ethanol and 2 mL of hydrochloric acid (37%) to remove the template. After 24 h of agitation at 50 °C, the solid was filtered and thoroughly washed with absolute ethanol. The same procedure was repeated three times. The resulting solid was first desiccated and then subjected to grafting of mercaptopropyl linkers. A 1.0 g portion of solid was suspended with 1.5 mL (7.9 mmol) of MPTMS in 20 mL of anhydrous toluene and stirred under refluxing for 24 h in an inert atmosphere. A 0.5 g portion of 9-amino(9-deoxy)epiquinine or 9-thiourea epiquinine and 1.0 g of grafted mercaptopropyl-derived mesoporous silicas were suspended in 25 mL of chloroform under N₂ atmosphere. After 30 min of agitation (to drive off the residual air in the suspension), 50 mg of azobisisobutyronitrile was added. After 24 h of agitation at 65 °C under inert atmosphere, the solid was filtered; washed thoroughly with chloroform, hexane, acetone, and absolute ethanol; and finally, dried under vacuum to give the immobilized catalysts.

In the asymmetric Michael addition reaction of nitromethane with chalcone, a molar ratio of chalcone/nitromethane/catalyst of 1/4/0.1 was applied. Typically, to a suspension mixture of chalcone and heterogeneous catalyst (~50 mg) in 0.5 mL of toluene, nitromethane was introduced in one portion. The mixture was oscillated at 30 °C for 120 h and then filtered. The filtrate was subjected to flash chromatography (silica gel with ethyl acetate/hexane = 1/8) to afford the desired product as well as the unconverted chalcone. The conversion was calculated as the molar percentage of the reacted to the total chalcone. The yield and ee were determined on the basis of the isolated product. The enantiomeric excess (ee) was determined by HPLC with a Daicel Chiralcel AD-H column on Varian Prostar 210 HPLC with a Prostar 325 UV–vis detector. The mobile phase was a mixture of hexane and *i*-PrOH (*v/v* = 80/20) at a flow rate of 1.0 mL/min.

2.2. Characterization. X-ray powder diffraction (XRD) patterns were obtained on a Rigaku D/MAX-2500 X-ray diffractometer operated at 45 kV and 40 mA using Cu K α radiation ($\lambda = 1.5418 \text{ \AA}$). The data were collected from 0.5 to 5° (2θ) with a resolution of 0.02°. N₂ sorption isotherms were measured on a Quantachrome Autosorb-1 system. The specific surface area was calculated using the Brunauer–Emmett–Teller (BET) method based on the adsorption branch. The pore size distribution was calculated using the Barrett–Joyner–Halenda method based on the adsorption branch. The single point pore volume was estimated from the adsorbed amount at $p/p_0 = 0.99$. In the α_s -plot analysis, nonporous α -quartz with a BET surface area of 1.21 m² g⁻¹ was employed as the reference. Elemental analyses were performed on a Bruker CHNS elemental analyzer. FT-IR spectra were taken on a Bruker Vector 22 spectrometer (resolution 4 cm⁻¹) in the range of 4000–400 cm⁻¹ using the standard KBr method. The solid state NMR experiments were carried out at resonance frequencies of 75.5 MHz for ¹³C MAS NMR and 59.6 MHz for ²⁹Si MAS NMR on a Bruker Avance 300 M solid-state spectrometer equipped with a commercial 5 mm MAS NMR probe. The magic-angle spinning frequencies were set to 5 kHz for all experiments. ¹H NMR in CDCl₃ were recorded on a Bruker Avance 600 spectrometer running at 600 MHz. Data for ¹H NMR are recorded as follows: chemical shift (δ , ppm),

multiplicity (s, singlet; d, doublet; t, triplet; q, quartet; m, multiplet), integration, coupling constant (Hz). Chemical shifts are reported in the δ scale relative to residual CHCl_3 (7.26 ppm). Molecular mass was determined on a micromass LCT spectrometer using electrospray (ES^+) ionization techniques.

2.3. Computational Details. The heterogeneous system model was based on quantum-mechanical/molecular-mechanical (QM/MM) calculations.⁴³ QM parts included the reactants and catalyst, and MM parts involved the linker and silica wall. Silicon atoms in the silica wall were saturated by three oxygen atoms at the inner surface and a hydrogen atom at the outer surface. The linker was assumed to attach to the silica wall via the linkage of the silicon atom to three oxygen atoms in the wall. To avoid deformation of the model, MM parts were frozen while QM parts were allowed to move to their equilibrium positions. In our research, a two-layer ONIOM protocol was used to couple the QM and MM parts. The semiempirical AM1 method⁴⁴ was used for QM calculations, and the UFF force field was used for MM potential calculations.

The semiempirical method hypothesizes that the optimized geometries in this reaction system are the same as those calculated by the accurate methods. To justify this hypothesis, immobilizing 9-thiourea epiquinine in the 7.7 nm mesopore, the transition states (S)-TS_{1-7.7} and (R)-TS_{1-7.7} are optimized by the HF/6-31G(d):UFF method. The results show that the geometries change trivially after HF/6-31G(d):UFF is calculated; i.e., N–H...O₂N in (S)-TS_{1-7.7} bond lengths change by <0.04 Å, and bond angles change by <8°; N–H...O=C in (S)-TS_{1-7.7} bond lengths are 2.00 and 1.95 Å (2.06 and 2.09 Å, respectively, by AM1:UFF). Furthermore, the energy difference also changes only slightly. The energy gap between (S)-TS_{1-7.7} and (R)-TS_{1-7.7} increases by 0.18 kJ/mol after optimization by the HF/6-31G(d):UFF method, which is very close to the energy calculated by the AM1:UFF method. Thus, neither the structures nor free energies are sensitive to the geometry optimization method. Because the semiempirical AM1 method is much less CPU-demanding, we base our further discussions only on the AM1 method for QM calculations. The transition state geometries were obtained by the QST2 method. For the homogeneous system, the semiempirical AM1 method was used. All calculations were performed with the quantum chemical program packages Gaussian 03.⁴⁵

3. RESULTS

3.1. Catalysts Preparation and Characterizations. The catalysts to be used here as model systems are 9-amino(9-deoxy)epiquinine or 9-thiourea epiquinine immobilized at the interior surfaces of mesoporous supports. The immobilization has been achieved by the step-by-step covalent linking approach shown in Figure 1.

The step-by-step fabrication of heterogeneous catalysts was monitored by ²⁹Si and ¹³C CP/MAS solid-state NMR spectra, FT-IR spectrum, N₂ adsorption–desorption experiments, XRD, and element analysis techniques. To ensure the active centers all anchored inside the mesoporous channels, the exterior surfaces of the mesoporous supports were first sheltered with –Si(CH₃)₃ moieties before exposure of the interior surfaces.

In the ²⁹Si CP/MAS NMR spectra shown in Figure 2, a visible resonance at 14 ppm appears, which is absent for the pristine mesoporous support. According to the previous study,⁴⁶ this resonance originates from the Si atoms in Si(CH₃)₃ grafted. The resonances at –90, –100, and –110 ppm

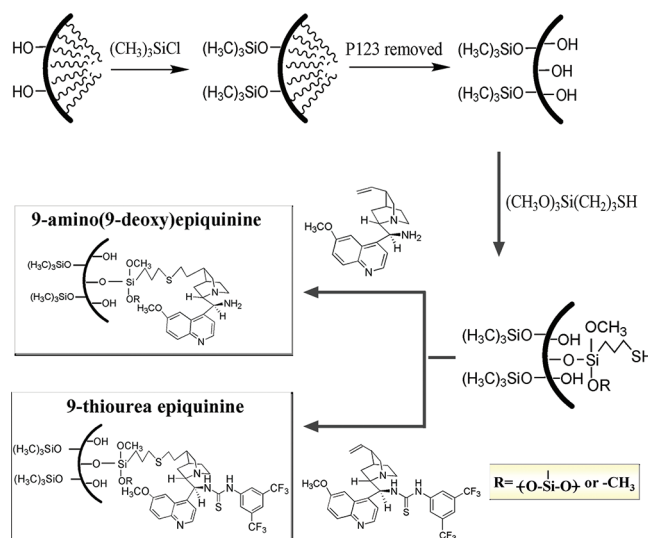


Figure 1. 9-Amino(9-deoxy)epiquinine and 9-thiourea epiquinine anchored inside the channels of the mesoporous supports.

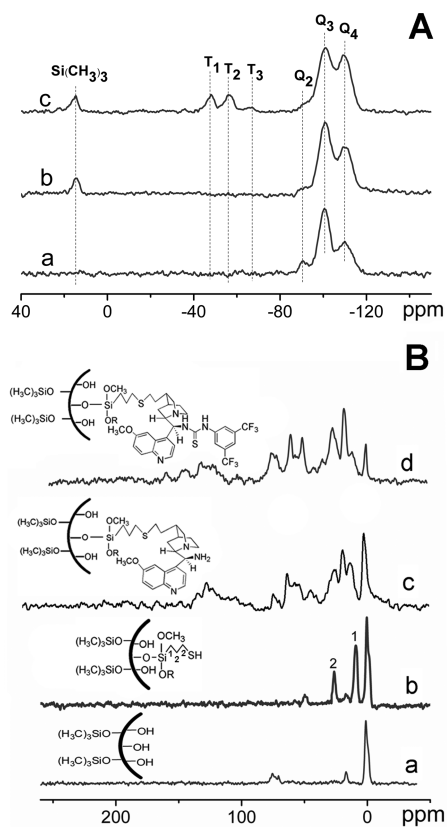


Figure 2. (A) ²⁹Si CP/MAS NMR spectra of (a) pristine, (b) exterior surface-sheltered, and (c) –SH grafted samples; (B) ¹³C CP/MAS NMR spectra of (a) exterior surface sheltered, (b) –SH grafted, (c) 9-amino(9-deoxy)epiquinine-immobilized, and (d) 9-thiourea epiquinine-immobilized samples.

associated with Q₂, Q₃, and Q₄ [$Q_n = \text{Si}(\text{OSi})_n(\text{OR})_{4-n}$, $n = 2-4$] are observed. Although the CP technique is limited in a quantification of peaks, the change of the peak intensities may allow giving a trend of the condensation degree in this work.^{47,48} The relative intensity of Q⁴ at –110 ppm to Q³ at –100 ppm presents a marked increase, and the resonance intensity of Q² linkage decreases. With the following grafting of

Table 1. Textural and Chemical Properties of Support Materials and Immobilized Catalysts

pore size of support ^c (nm)	support	immobilized QN ^a						immobilized SQT ^b				
		S_{ex} (m ² /g) ^d	S_{p} (m ² /g) ^e	S_{t} (m ² /g) ^f	S_{t} (m ² /g) ^f	pore size (nm)	content of QN (mmol/g)	density of QN (/nm ²)	S_{t} (m ² /g)	pore size (nm)	content of SQT (mmol/g)	density of SQT (/nm ²)
4.7	sheltered	86	854	940	613	3.6	0.034	0.03	532	3.3	0.063	0.07
	-SH grafted	90	767	857								
5.8	sheltered	46	448	494	184	4.9	0.204	0.67				
	-SH grafted	45	367	412								
6.3	sheltered	42	468	510	167	5.4	0.152	0.55	190	5.5	0.156	0.49
	-SH grafted	38	268	306								
7.3	sheltered	29	553	582					524	6.4	0.060	0.07
	-SH grafted	26	543	569								
9.8	sheltered	60	422	482	255	8.0	0.066	0.14				
	-SH grafted	60	352	412								
10.7	sheltered	67	578	645					345	8.9	0.156	0.27
	-SH grafted	70	389	459								
11.3	sheltered	57	399	456					348	9.7	0.061	0.11
	-SH grafted	61	372	433								

^aQN: 9-amino(9-deoxy)epiquinine. ^bSQT: 9-thiourea epiquinine. ^cSheltered support with -Si-(CH₃)₃. ^d S_{ex} : specific areas of exterior surface. ^e S_{p} : specific areas of interior surface. ^f $S_{\text{t}} = S_{\text{ex}} + S_{\text{p}}$.

mercaptopropylsilyl moiety, the relative intensity of Q⁴ to Q³ further increases, and the Q² resonance becomes hardly observed. Simultaneously, the resonances at -48, -56, and -67 ppm associated with T₁, T₂ and T₃ linkages ($T_m = \text{RSi}(\text{OSi})_m(\text{OCH}_3)_{3-m}$, $m = 1-3$) are well resolved, verifying the anchor of mercaptopropyl groups to silica walls.

In the ¹³C CP/MAS NMR spectra (Figure 2), the mesoporous support with exterior surface sheltered clearly displays a resonance at 1.50 ppm, which originates from the grafted Si-(CH₃)₃. The following modification with mercaptopropyl groups gives rise to three new resonances at 10, 27, and 49 ppm, which is consistent with that previously resolved.⁴⁹ The resonances at 10 and 27 ppm are assigned to the Si-CH₂- and CH₂-CH₂-SH of the tethered mercaptopropyl moieties. The resonance at 48 ppm arises from the residual methoxy groups due to the incomplete condensation of 3-mercaptopropyltrimethoxysilane. To make clear the location of grafted mercaptopropyl moieties, α_s -plot analysis⁵⁰ has been performed (see Table 1). In each case, the mercaptopropyl grafting causes a marked decrease in the specific area of interior surface while the specific area of exterior surface hardly changes. It confirms that the grafting of mercaptopropyl groups has occurred only at the interior surface, just as rationally predicted. According to the calculations from the surface areas and the content of the active centers, the distribution of the catalytic centers in the support cavity can be obtained which supposes the active centers exist as isolated single sites.

Reaction of the mercaptopropyl-modified mesoporous surface with 9-amino(9-deoxy)epiquinine or 9-thiourea epiquinine yields the immobilized catalysts. The introduction of catalytic centers results in a decrease in the specific surface area. The more the catalytic centers are incorporated, the more the surface areas decrease (see Table 1), but all the resulting heterogeneous catalysts retain the well-defined mesoporous structure typical of long-range ordered hexagonal symmetry. In

the XRD patterns (not shown here), well-resolved (100), (110), and (200) reflections are clearly observed in all cases. In the FT-IR spectra (see Figure 3), the IR absorption band at 2576 cm⁻¹, arising from S-H vibration, vanishes due to the covalent combination of catalytic centers. The absorption band at 1278 cm⁻¹ arises from the C=S bond vibration. The

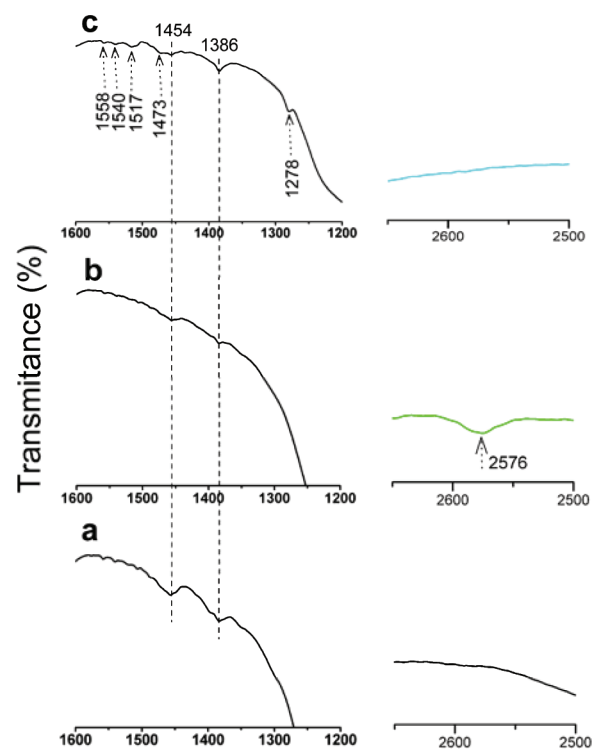


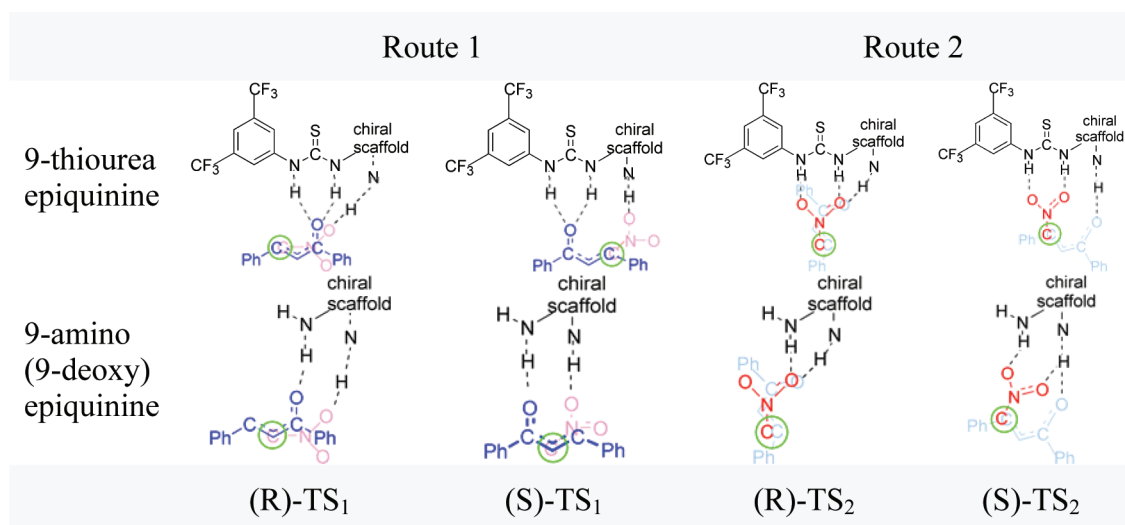
Figure 3. FT-IR spectra of (a) sheltered support, (b) grafted support, and (c) immobilized 9-thiourea epiquinine.

Table 2. Experimental Results for the Asymmetric Michael Addition Reaction of Nitromethane and Chalcone^a

pore size (nm)	9-amino(9-deoxy)epiquinine			pore size (nm)	9-thiourea epiquinine		
	conversion (%)	yield (%)	ee (%)		conversion (%)	yield (%)	ee (%)
<i>b</i>	61	56	76 (<i>S</i>)	<i>b</i>	71	64	94 (<i>R</i>)
4.7	29 (25)	21 (18)	57 (54)	4.7	25 (23)	22 (20)	75 (73)
5.8	44 (43)	35 (32)	38 (33)	6.3	66 (65)	63 (59)	93 (92)
6.3	39 (34)	29 (25)	23 (21)	7.3	63 (64)	59 (61)	85 (82)
9.8	25 (24)	18 (15)	12 (10)	10.7	61 (61)	58 (58)	69 (65)
				11.3	58 (56)	55 (53)	39 (38)

^aReactions were carried out with 4.0 mmol of nitromethane, 1.0 mmol of chalcone, and 10 mol % of catalytic site in 0.50 mL of toluene for 120 h.

^bHomogeneous catalysis. The figures in the parentheses are reproduced results.

Scheme 1. Competing Hydrogen-Bonding Activation Routes to the *R* and *S* Transition States

absorption bands assigned to symmetric (δ_s) and asymmetric (δ_{as}) vibrations of $-\text{CH}_3$ in $-\text{Si}(\text{CH}_3)_3$ grafted on the exterior surface are observed at 1386 and 1456 cm^{-1} . The IR bands at 1558, 1540, 1512, and 1473 cm^{-1} , all originating from the bone vibrations ($\nu_{\text{C}=\text{C}}$) of aryl rings, and the ^{13}C resonances at 33 ($\text{Si}-(\text{CH}_2)_3-\text{S}-\text{CH}_2-\text{CH}_2-$); 50 ($\text{O}-\text{CH}_3$); 26, 41, 55, 59 (quinidine); and 101, 121, 131, 143, 158 (aromatic carbons), all characteristic of 9-amino(9-deoxy)epiquinine or 9-thiourea epiquinine, are clearly observed.

3.2. Enantioselective Michael Addition between Nitromethane and Chalcone. The products of the enantioselective Michael addition between nitromethane and chalcone are useful intermediates for a variety of further elaborated structures, such as chiral aminocarbonyls, pyrrolidines, γ -lactams, and γ -amino acids.^{51,52} Applied to the reaction, the catalysts give varied enantioselectivities, depending on either the pore size of the mesoporous support or the nature of the organocatalytic moiety. In a homogeneous system, 9-amino(9-deoxy)epiquinine catalyst produces an enantiomer excess of 76% with major *S* configuration, and 9-thiourea epiquinine catalyst produces an enantiomer excess of 94% with major *R* configuration. The immobilization of either 9-amino(9-deoxy)epiquinine or 9-thiourea epiquinine results in a reduced enantioselectivity, holding the same major configuration as homogeneous counterparts, as can be seen in Table 2. The experimental observations provide direct evidence for the great

challenge to the heterogeneous enantioselective organocatalysis. For both catalytic moieties, a gradual improvement of enantioselectivity with constricted pore size is observed. It means the chiral induction has been recovered by the restriction of organocatalytic moiety in mesoporous supports. The restriction by mesoporous channel makes a more positive impact on the asymmetric induction of 9-thiourea epiquinine than on 9-amino(9-deoxy)epiquinine. For 9-thiourea epiquinine, the enantiomer excess not only visibly increases with reduced pore size, but also reaches the level for a homogeneous counterpart (93% vs 94% ee) when the support pore size is reduced to 6.3 nm. That is, it is possible to achieve the confinement in the organocatalysis by rationally modulating the dimension of confined space, but when the pore size is further shrunk to 4.7 nm, the enantiomer excess is found to display a decrease instead (to 75% ee), suggesting that the confinement requires an optimized spatial dimension.

4. DISCUSSION

4.1. Theoretical Exploration of Favored Transition States. Cinchona-derived thiourea has been recognized as a bifunctional organocatalyst⁵³ capable of activating simultaneously both nucleophile and electrophile. In the Michael addition reaction of nitromethane and chalcone, nitroalkane acts as a nucleophile, and chalcone acts as an electrophile. The

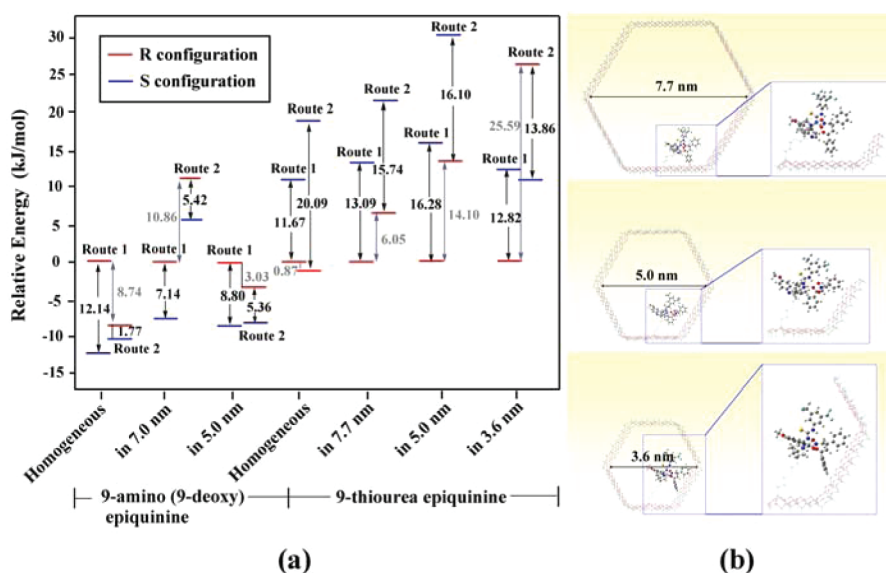


Figure 4. (a) Relative energy profile of competing hydrogen-bonding activation routes to *R* and *S* transition states and (b) computational models for heterogeneous 9-thiourea epiquinine as examples.

activation is proposed to operate through two hydrogen-bonding activation competitive routes (routes 1 and 2 in Scheme 1). Route 1 represents nucleophile activation by the protonated amine group and electrophile activation by the thiourea moiety, and route 2 represents the opposite activated mechanism. On the homogeneous 9-thiourea epiquinine, the energy of the *S* transition state, which represents the transition state leading to the *S* configuration product, is predicted to be notably higher for both routes 1 and 2 than that of the *R* transition state, which represents the transition state leading to the *R* configuration product (Figure 4). In route 1, (*S*)-TS₁ is 11.67 kJ/mol less favored than (*R*)-TS₁, whereas on the alternative route, (*S*)-TS₂ is found to be 20.09 kJ/mol less stable than (*R*)-TS₂, so either pathway is predicted to lead to the *R* major enantiomeric form. Experimentally, an enantiomer excess of 94% with major *R* configuration has been observed. The calculation results and experimental observations agree well with each other. At the same time, (*R*)-TS₂ is predicted to be 0.87 kJ/mol lower in energy than (*R*)-TS₁ (Figure 4).

The results suggest that, for the Michael addition reaction catalyzed by homogeneous 9-thiourea epiquinine, route 2 represents an energetically preferred pathway to give the major *R* configuration. A previous work based on density functional theory calculation⁵⁴ has indicated that the complex corresponding to the coordination of the electrophilic species to thiourea is less stable than the complex formed on the alternative route, which is entirely consistent with our results.

For 9-amino(9-deoxy)epiquinine, the hydrogen-bonding activation route 1 represents nucleophile activation by the protonated amine group and electrophile activation by the primary amine, and route 2 represents the opposite activated mechanism, but another competitive activation model, enamine activation, has to be taken into considerations,^{55–57} so the energies of the transition states corresponding to both activation models have been calculated. The enamine activation is predicted to be notably higher in energy (2532.29 kJ/mol for (*R*)-TS and 2545.95 kJ/mol for (*S*)-TS) than hydrogen-bonding activation (2262.39 kJ/mol for (*R*)-TS₁ and 2250.32 kJ/mol for (*S*)-TS₁; 2253.73 kJ/mol for (*R*)-TS₂ and 2251.89 kJ/mol for (*S*)-TS₂). The results indicate that the hydrogen-

bonding activation is energetically preferred to enamine activation.

According to the calculation results on the catalysis of homogeneous 9-amino(9-deoxy)epiquinine via hydrogen-bonding activation (Figure 4), the energy of (*R*)-TS, which represents the transition state leading to the *R* configuration product, is notably higher in both hydrogen-bonding activation routes. Either pathway is predicted to lead to the major *S* enantiomeric form. For route 1, (*R*)-TS₁ is calculated to be 12.14 kJ/mol less favored than (*S*)-TS₁, and on the alternative route, this gap decreases to 1.77 kJ/mol. (*S*)-TS₁ is calculated to be 1.63 kJ/mol lower in energy than (*S*)-TS₂. The results suggest that, for the Michael addition reaction catalyzed by homogeneous 9-amino(9-deoxy)epiquinine, the hydrogen-bonding activation by route 1 is an energetically preferred pathway to give the major *S* configuration. Experimentally, an enantiomer excess of 76% with major *S* configuration has been observed, which is consistent with the theoretical prediction (Figure 5), but the energy calculation based on the enamine activation mechanism indicates that (*R*)-TS is 13.65 kJ/mol more stable than (*S*)-TS, which is in contrast to the experimental observation of *S* enantiomer excess.

4.2. Dependence of Transition States on the Pore Size. The heterogeneous models are established as shown in

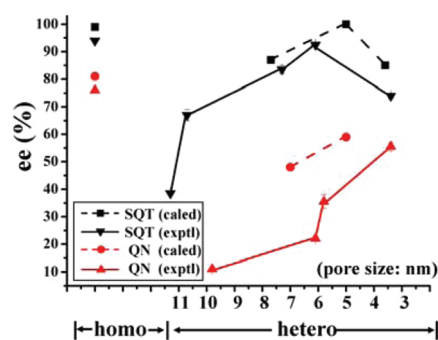


Figure 5. Graph of experimental ee versus calculated values for the reaction.

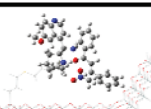
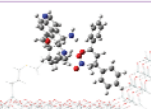
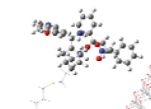

Figure 4b to investigate the effects of immobilization on the transition state energies. The calculated energies are also summarized in Figure 4 (see Supporting Information Tables S3 and S4 for detailed optimal geometries). Immobilizing 9-amino(9-deoxy)epiquinine in the support with a pore size of 7.0 nm, the energy gap between the *R* and *S* transition states in route 1 is calculated to decrease from 12.14 to 7.14 kJ/mol, representing a reduced ee value experimentally observed after immobilization (Figure 5). The energy gap between the *R* and *S* transition states in route 2 increases from 1.77 to 5.42 kJ/mol, but the heterogeneous 9-amino(9-deoxy)epiquinine still produces a major *S* configuration via route 1, just as the homogeneous counterpart. Immobilizing 9-thiourea epiquinine in the 7.7 nm mesopore, the activation route is switched to route 1 according to the calculation results on the transition state energies, rather than route 2, which is favored in the homogeneous system. Although the energy difference between the *S* and *R* transition states in route 1 has been enlarged to 13.09 kJ/mol from 11.67 kJ/mol by the immobilization, it is smaller than the energy gap of route 2 in the homogeneous system, accounting for the reduction of ee experimentally observed (Figure 5).

The dependence of the transition state energy on the pore size has been further explored in this work. As can be seen from Figure 4, for the immobilized 9-amino(9-deoxy)epiquinine, the energy gap between the *R* and *S* transition states in the energetically favored route 1 increases by 1.66 kJ/mol when the pore size is reduced from 7.0 to 5.0 nm. The enlarged energy difference leads to an improved ee value, as observed in the experiment. For the immobilized 9-thiourea epiquinine, the energy gap between the *S* and *R* transition states increases by 3.19 kJ/mol when the pore size is reduced from 7.7 to 5.0 nm, preserving route 1 as the energetically favored pathway. The enlarged energy gap between *S* and *R* transition states accounts for the enhanced ee value (Figure 5). Further reducing the pore size, for example, to 3.6 nm, the energy gap between *S* and *R* transition states decreases instead to 12.82 kJ/mol, 3.46 kJ/mol below the energy barrier between (*S*)-TS₁-5.0 and (*R*)-TS₁-5.0, which accounts for the decreased ee value observed in the experiment.

It should be pointed out that the modulation of pore size also has an impact on the competitive route. For example, in the 9-thiourea epiquinine systems, the reduction of pore size from 7.7 to 5.0 nm enlarges the energy difference between routes 2 and 1 from 6.05 to 14.10 kJ/mol, making route 2 less competitive. The *R* and *S* transition states are reversed in energy for route 2 when the pore size decreases to 3.6 nm, accompanied by an energy difference between the *R* and *S* transition states (13.86 kJ/mol), but no evidence directly illuminates whether the energy gap between the two competitive activation routes contributes to the enantioselectivity in that no switch of the activation routes has occurred.

4.3. Hydrogen-Bonding between the Pore Wall and Substrates Analyzed. As discussed above, the changes in the energy gaps between the *R* and *S* transition states have well explained the dependence of enantioselectivity on the pore size in the heterogeneous organocatalysis via hydrogen-bonding activation. This is supposed to be related virtually to the hydrogen bonds between the pore wall and substrates. The optimized hydrogen-bonding networks between the substrate and the pore wall are illustrated in Tables 3 and 4 by using the AM1 method. As can be explored from Table 3, decreasing the pore size of heterogeneous 9-amino(9-deoxy)epiquinine

Table 3. Optimized Hydrogen-Bonding Interactions between Substrate and Pore Wall in the Catalysis of 9-Amino(9-deoxy)epiquinine

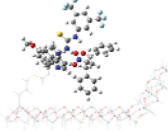

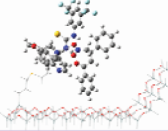
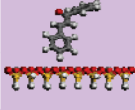
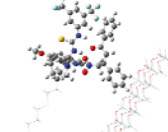
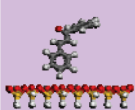
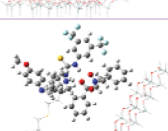
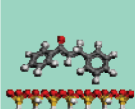
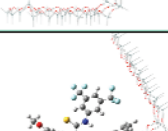
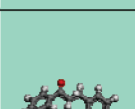
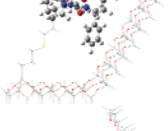
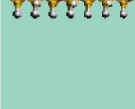
Pore size (nm)	TS for favored route	Interaction between substrate and pore wall	Hydrogen bond		
			N	Distance range (Å)	Angle range (degree)
7.0	S		3	2.61-2.73	124-137
	R		3	2.52-3.04	113-125
5.0	S		2	2.65-2.91	122-124
	R		3	2.81-3.12	102-104

catalyst from 7.0 to 5.0 nm breaks one hydrogen bond from the pore wall to the substrate in the *S* configuration activation. That is, there is one more hydrogen bond between the pore wall and the substrate in (*R*)-TS₁-5.0 than in (*S*)-TS₁-5.0, but the C–H...O–Si hydrogen bond in (*S*)-TS₁-5.0 is stronger than in (*R*)-TS₁-5.0 (2.65 vs 2.81 Å). So there is actually no prominent difference between the interactions with pore wall for both the *R* and *S* transition states. The results indicate the influence of the shrunk pore size represents only a slight increase in the energy difference between the *S* and *R* transition states.

As can be explored from Table 4, reducing the pore size of heterogeneous 9-thiourea epiquinine from 7.7 to 5.0 nm, the hydrogen-bonding interactions of the substrate with pore wall are strengthened for the *R* transition state. The C–H...O–Si hydrogen bonds in (*R*)-TS₁-5.0 increase to complex five from simple three-dentate in (*R*)-TS₁-7.7. The hydrogen bonds between the substrate and the pore wall in (*S*)-TS₁-5.0 seem no different from (*S*)-TS₁-7.7 and may lead to an enlargement of the energy difference between the *R* and *S* transition states of route 1. Further reduction of the pore size to 3.6 nm is accompanied by the changes in the hydrogen-bonding interactions between the substrate and the pore wall, as can be seen in Table 4. The hydrogen-bonding interactions between the substrate and the pore wall in (*S*)-TS₁-3.6 turn to a five-dentate hydrogen-bonding network, approaching the same number as in (*R*)-TS₁-3.6. This change in the hydrogen bonds from the pore wall may further lead to a reduction in the energy gap between (*R*)-TS₁-3.6 and (*S*)-TS₁-3.6. The hydrogen-bonding interactions between chalcone and the pore wall in the case of (*S*)-TS₂-3.6 in route 2 change to five C–H...O–Si bonds, but in the *R* isomer, there are still three, reversing the relative energy for the *R* and *S* transition states.

It should be made clear that, although the polarizable continuum models have been widely used to estimate the

Table 4. Optimized Hydrogen-Bonding Interactions between Substrate and Pore Wall in the Catalysis of 9-Thiourea Epiquinine

Pore size (nm)	TS for favored route	Interaction between substrate and pore wall	Hydrogen bond			
			N	Distance range (Å)	Angle range (degree)	
7.7	S			3	2.71-2.95	118-149
	R			3	2.68-2.89	114-119
5.0	S			3	2.65-2.78	116-144
	R			5	2.68-2.94	119-146
3.6	S			5	2.61-2.80	110-166
	R			5	2.69-3.10	108-114

solvation of the reaction components, their estimation for hydrogen-bonded interactions always deviates notably from the real ones.⁵⁴ So in this work, toluene molecules were added into the calculated model directly until the optimized energy remained stable. According to the volume of heterogeneous model (18 Å × 18 Å × 8 Å) and the density and molecular weight of toluene, the number of toluene molecules has been estimated to be not more than 14. The calculation indicates the energy surface turns to complanation when 10 solvent molecules have been introduced (see Supporting Information Figure S1). Taking route 2 in the catalysis of 9-thiourea epiquinine as an example, it is found that the energy difference between the *R* and *S* transition states in the system with optimized solvent molecules (20.01 kJ/mol) is similar to that without a solvent molecule (21.13 kJ/mol). Comparing the energy of the heterogeneous system with the solvent molecules in the optimized number and without solvent molecules (54825.69 kJ/mol versus 54637.44 kJ/mol), it can be concluded that the interactions between the support surface

as host and the substrate molecules as guest prove the top priority to the solvent effects. So our calculations and discussions have all been carried out on the basis of gas-phase energies.

5. CONCLUSIONS

In summary, cinchona alkaloid-derived 9-amino(9-deoxy)-epiquinine and 9-thiourea epiquinine have been immobilized at the interior surface of mesoporous hosts in this work to explore the dependence of organocatalytic enantioselectivity on the interaction between the substrate and the pore wall. With rationally modulating the pore size of mesoporous hosts, it has been demonstrated that the confinement can be experimentally achieved in the heterogeneous Michael addition of nitromethane and chalcone. For 9-amino(9-deoxy)epiquinine, enantiomer excess improvement has been observed with constricted pore size. For 9-thiourea epiquinine, the enantioselectivity not only visibly increases with reduced pore size, but also reaches the level for homogeneous counterpart when the support pore size is reduced to 6.3 nm. Theoretical calculations on the energy gaps between the *R* and *S* transition states have well explained the dependence of enantioselectivity on the pore size. For the Michael addition reaction catalyzed by 9-thiourea epiquinine, the relative error between the computational and the experimental ee values is lower than 25%. The optimized hydrogen-bonding interaction analysis reveals that the hydrogen bonds between the pore wall and substrates modify the energy gap between the *S* and *R* transition states or even switch the competitive activation routes. The main findings of this work are expected to extend the understanding of the essence of confinement in asymmetric synthesis and further assist in designing efficient enantioselective catalysts.

■ ASSOCIATED CONTENT

📄 Supporting Information

¹H NMR data, HPLC data, computational solvent effects, Cartesian coordinates, and absolute energies of all transition states. This material is available free of charge via the Internet at <http://pubs.acs.org/>.

■ AUTHOR INFORMATION

✉ Corresponding Author

*Phone: +86-10-6442 5280. Fax: +86-10-6442 5385. E-mail: jinghe@263.net.cn.

📝 Notes

The authors declare no competing financial interest.

■ ACKNOWLEDGMENTS

The authors are grateful for financial support from the NSFC, "973" Program (2011CBA00504) and the Scientific Research Foundation of the Graduate School of Beijing University of Chemical and Technology. J.H. particularly appreciates the financial aid of the China National Funds for Distinguished Young Scientists from the NSFC.

■ REFERENCES

- (1) Thomas, J. M.; Johnson, B. F. G.; Raja, R.; Sankar, G.; Midgley, P. A. *Acc. Chem. Res.* **2003**, *36*, 20–30.
- (2) Caplan, N. A.; Hancock, F. E.; Page, P. C. B.; Hutchings, G. J. *Angew. Chem., Int. Ed.* **2004**, *43*, 1685–1688.
- (3) Rase, H. F. *Handbook of Commercial Catalysts: Heterogeneous Catalysts*; CRC Press: New York, 2000.

- (4) Vankelecom, I.; Wolfson, A.; Geresh, S.; Landau, M.; Gottlieb, M.; Hershkovitz, M. *Chem. Commun.* **1999**, 2407–2408.
- (5) Pini, D.; Mandoli, A.; Orlandi, S.; Salvadori, P. *Tetrahedron: Asymmetry* **1999**, *10*, 3883–3886.
- (6) Annunziata, R.; Benaglia, M.; Cinquini, M.; Cozzi, F.; Pitillo, M. J. *Org. Chem.* **2001**, *66*, 3160–3166.
- (7) Hallman, K.; Moberg, C. *Tetrahedron: Asymmetry* **2001**, *12*, 1475–1478.
- (8) Fraile, J. M.; García, J. I.; Harmer, M. A.; Herrerías, C. I.; Mayoral, J. A. *J. Mol. Catal. A: Chem.* **2001**, *165*, 211–218.
- (9) Johnson, B. F. G.; Raynor, S. A.; Shephard, D. S.; Mashmeyer, T.; Thomas, J. M.; Sankar, G.; Bromley, S.; Oldroyd, R.; Gladdenc, L.; Mantle, M. D. *Chem. Commun.* **1999**, 1167–1168.
- (10) Raja, R.; Thomas, J. M. *J. Mol. Catal. A: Chem.* **2002**, *181*, 3–14.
- (11) Xiang, S.; Zhang, Y.; Xin, Q.; Li, C. *Chem. Commun.* **2002**, 2696–2697.
- (12) Kureshy, R. I.; Ahmad, I.; Khan, N. H.; Abdi, S. H. R.; Singh, S.; Pandia, P. H.; Jasra, R. V. *J. Catal.* **2005**, *235*, 28–34.
- (13) Lou, L.-L.; Yu, K.; Ding, F.; Peng, X.; Dong, M.-M.; Zhang, C.; Liu, S. *J. Catal.* **2007**, *249*, 102–110.
- (14) Zhou, X.; Yu, X.; Huang, J.; Li, S.; Li, L.; Che, C. *Chem. Commun.* **1999**, 1789–1790.
- (15) Jones, M. D.; Raja, R.; Thomas, J. M.; Johnson, B. F. G.; Lewis, D. W.; Rouzaud, J.; Harris, K. D. M. *Angew. Chem., Int. Ed.* **2003**, *42*, 4326–4331.
- (16) Raja, R.; Thomas, J. M.; Jones, M. D.; Johnson, B. F. G.; Vaughan, D. E. W. *J. Am. Chem. Soc.* **2003**, *125*, 14982–14983.
- (17) Thomas, J. M.; Maschmeyer, T.; Johnson, B. F. G.; Shephard, D. S. *J. Mol. Catal. A: Chem.* **1999**, *141*, 139–144.
- (18) Li, C. *Catal. Rev.* **2004**, *46*, 419–492.
- (19) Clarke, R. J.; Shannon, I. J. *Chem. Commun.* **2001**, 1936–1937.
- (20) Bigi, F.; Moroni, L.; Maggi, R.; Sartori, G. *Chem. Commun.* **2002**, 716–717.
- (21) Yu, K.; Gu, Z.; Ji, R.; Lou, L.; Ding, F.; Zhang, C.; Liu, S. *J. Catal.* **2007**, *252*, 312–320.
- (22) Yu, K.; Gu, Z.; Ji, R.; Lou, L.; Liu, S. *Tetrahedron* **2009**, *65*, 305–311.
- (23) Kureshy, R. I.; Ahmad, I.; Khan, N. H.; Abdi, S. H. R.; Pathak, K.; Jasra, R. V. *Tetrahedron: Asymmetry* **2005**, *16*, 3562–3569.
- (24) Kureshy, R. I.; Ahmad, I.; Khan, N. H.; Abdi, S. H. R.; Singh, S.; Pandia, P. H.; Jasra, R. V. *J. Catal.* **2006**, *238*, 134–141.
- (25) Zhang, H.; Xiang, S.; Li, C. *Chem. Commun.* **2005**, 1209–1211.
- (26) Zhang, H.; Zhang, Y.; Li, C. *J. Catal.* **2006**, *238*, 369–381.
- (27) Zhang, H.; Wang, Y.; Zhang, L.; Gerritsen, G.; Abbenhuis, H. C. L.; van Santen, R. A.; Li, C. *J. Catal.* **2008**, *256*, 226–236.
- (28) Doyagüez, E. G.; Calderón, F.; Sánchez, F.; Fernández-Mayoralas, A. J. *Org. Chem.* **2007**, *72*, 9353–9356.
- (29) Corma, A.; Iborra, S.; Rodríguez, I.; Iglesias, M.; Sánchez, F. *Catal. Lett.* **2002**, 237–242.
- (30) Prasetyanto, E. A.; Lee, S.-C.; Jeong, S.-M.; Park, S.-E. *Chem. Commun.* **2008**, 1995–1997.
- (31) Benaglia, M.; Puglisi, A.; Cozzi, F. *Chem. Rev.* **2003**, *103*, 3401–3429.
- (32) Dalko, P. I.; Moisan, L. *Angew. Chem., Int. Ed.* **2001**, *40*, 3726–3748.
- (33) Gaunt, M. J.; Johansson, C. C. C.; McNally, A.; Vo, N. T. *Drug Discovery Today* **2007**, *12*, 8–27.
- (34) Sibi, M. P.; Manyem, S. *Tetrahedron* **2000**, *56*, 8033–8061.
- (35) Krause, N.; Hoffmann-Röder, A. *Synthesis* **2001**, 171–196.
- (36) Christoffers, J.; Baro, A. *Angew. Chem., Int. Ed.* **2003**, *42*, 1688–1690.
- (37) Schreiner, P. R. *Chem. Soc. Rev.* **2003**, *32*, 289–296.
- (38) MacMillan, D. W. C. *Nature* **2008**, *455*, 304–308.
- (39) Yu, P.; He, J.; Guo, C. *Chem. Commun.* **2008**, 2355–2357.
- (40) Vakulya, B.; Varga, S.; Csámpai, A.; Soós, T. *Org. Lett.* **2005**, *7*, 1967–1969.
- (41) Monnier, A.; Schüth, F.; Huo, Q.; Kumar, D.; Margolese, D.; Maxwell, R. S.; Stucky, G. D.; Krishnamurthy, M.; Petroff, P.; Firouzi, A.; Janicke, M.; Chmelka, B. F. *Science* **1993**, *261*, 1299–1303.
- (42) Zhao, D.; Feng, J.; Huo, Q.; Melosh, N.; Fredrickson, G. H.; Chmelka, B. F.; Stucky, G. D. *Science* **1998**, *279*, 548–552.
- (43) Marti, S.; Moliner, V. J. *Chem. Theory Comput.* **2005**, *1*, 1008–1016.
- (44) Dewar, M. J. S.; Zoebisch, E. G.; Healy, E. F.; Stewart, J. J. P. *J. Am. Chem. Soc.* **1985**, *107*, 3902–3909.
- (45) Frisch, M. J.; Trucks, G. W.; Schlegel, H. B.; Scuseria, G. E.; Robb, M. A.; Cheeseman, J. R.; Montgomery, J. A., Jr.; Vreven, T.; Kudin, K. N.; Burant, J. C.; Millam, J. M.; Iyengar, S. S.; Tomasi, J.; Barone, V.; Mennucci, B.; Cossi, M.; Scalmani, G.; Rega, N.; Petersson, G. A.; Nakatsuji, H.; Hada, M.; Ehara, M.; Toyota, K.; Fukuda, R.; Hasegawa, J.; Ishida, M.; Nakajima, T.; Honda, Y.; Kitao, O.; Nakai, H.; Klene, M.; Li, X.; Knox, J. E.; Hratchian, H. P.; Cross, J. B.; Bakken, V.; Adamo, C.; Jaramillo, J.; Gomperts, R.; Stratmann, R. E.; Yazyev, O.; Austin, A. J.; Cammi, R.; Pomelli, C.; Ochterski, J. W.; Ayala, P. Y.; Morokuma, K.; Voth, G. A.; Salvador, P.; Dannenberg, J. J.; Zakrzewski, V. G.; Dapprich, S.; Daniels, A. D.; Strain, M. C.; Farkas, O.; Malick, D. K.; Rabuck, A. D.; Raghavachari, K.; Foresman, J. B.; Ortiz, J. V.; Cui, Q.; Baboul, A. G.; Clifford, S.; Cioslowski, J.; Stefanov, B. B.; Liu, G.; Liashenko, A.; Piskorz, P.; Komaromi, I.; Martin, R. L.; Fox, D. J.; Keith, T.; Al-Laham, M. A.; Peng, C. Y.; Nanayakkara, A.; Challacombe, M.; Gill, P. M. W.; Johnson, B.; Chen, W.; Wong, M. W.; Gonzalez, C.; Pople, J. A. *Gaussian 03, Revision C.02*; Gaussian, Inc.: Wallingford, CT, 2004.
- (46) Sindorf, D. W.; Maciel, G. E. *J. Am. Chem. Soc.* **1983**, *105*, 1848–1851.
- (47) Lelli, M.; Gajan, D.; Lesage, A.; Caporini, M. A.; Vitzthum, V.; Miéville, P.; Héroguel, F.; Rascón, F.; Roussey, A.; Thieuleux, C.; Boualleg, M.; Veyre, L.; Bodenhausen, G.; Copéret, C.; Emsley, L. *J. Am. Chem. Soc.* **2011**, *133*, 2104–2107.
- (48) Rossini, A. J.; Zagdoun, A.; Lelli, M.; Gajan, D.; Rascon, F.; Rosay, M.; Maas, W. E.; Copéret, C.; Lesage, A.; Emsley, L. *Chem. Sci.* **2012**, *3*, 108–115.
- (49) Dufaud, V.; Davis, M. E. *J. Am. Chem. Soc.* **2003**, *125*, 9403–9413.
- (50) Kruk, M.; Jaroniec, M. *Langmuir* **1997**, *13*, 6267–6273.
- (51) Ballini, R.; Bosica, G.; Fiorini, D.; Palmieri, A.; Petrini, M. *Chem. Rev.* **2005**, *105*, 933–972.
- (52) Corey, E. J.; Zhang, F. Y. *Org. Lett.* **2000**, *2*, 4257–4259.
- (53) Okino, T.; Hoashi, Y.; Furukawa, T.; Xu, X.; Takemoto, Y. *J. Am. Chem. Soc.* **2005**, *127*, 119–125.
- (54) Andrea, H.; Gábor, S.; Tibor, S.; Imre, P. *J. Am. Chem. Soc.* **2006**, *128*, 13151–13160.
- (55) Xie, J.; Chen, W.; Li, R.; Zeng, M.; Du, W.; Yue, L.; Chen, Y. *Angew. Chem., Int. Ed.* **2007**, *46*, 389–392.
- (56) Xie, J.; Yue, L.; Chen, W.; Du, W.; Zhu, J.; Deng, J.; Chen, Y. *Org. Lett.* **2007**, *9*, 413–415.
- (57) Tan, B.; Shi, Z.; Chua, P. J.; Zhong, G. *Org. Lett.* **2008**, *10*, 3425–3428.